A strong magnetic field in the jet base of a supermassive black hole

REFERENCES AND NOTES

1. G. Binnig, C. F. Quate, C. Gerber, *Phys. Rev. Lett.* **56**, 930–933 (1986).
2. F. J. Giessibl, S. Hembacher, H. Bielefeldt, J. Mannhart, *Science* **289**, 422–425 (2000).
3. H. J. Hug *et al.*, *Science* **291**, 2509a (2001).
4. F. J. Giessibl, H. Bielefeldt, S. Hembacher, J. Mannhart, *Ann. Phys.* **10**, 887–910 (2001).
5. M. Herz, F. J. Giessibl, J. Mannhart, *Phys. Rev. B* **68**, 045301 (2003).
6. A. N. Chaika, A. N. Myagkov, *J. Phys. Conf. Ser.* **100**, 012020 (2008).
7. S. Hembacher, F. J. Giessibl, J. Mannhart, *Science* **305**, 380–383 (2004).
8. J. Welker, F. J. Giessibl, *Science* **336**, 444–449 (2012).
9. T. Hofmann, F. Pielmeier, F. J. Giessibl, *Phys. Rev. Lett.* **112**, 066101 (2014).
10. M. Ternes, C. P. Lutz, C. F. Hirjibehedin, F. J. Giessibl, A. J. Heinrich, *Science* **319**, 1066–1069 (2008).
11. A. Zangwill, *Physics on Surfaces* (Cambridge Univ. Press, Cambridge 1988).
12. Submolecular resolution is defined as the ability to resolve atomic positions within molecules. Here, we refer to subatomic resolution as the ability to image single atoms as nontrivial features such as tori or multiple extrema, in contrast to single protrusions or single depressions.
13. L. Gross, F. Mohn, N. Moll, P. Liljeroth, G. Meyer, *Science* **325**, 1110–1114 (2009).
14. L. Bartels, G. Meyer, K. H. Rieder, *Appl. Phys. Lett.* **71**, 213 (1997).
15. L. Gross *et al.*, *Science* **337**, 1326–1329 (2012).
16. D. G. de Oteyza *et al.*, *Science* **340**, 1434–1437 (2013).
17. N. Moll, L. Gross, F. Mohn, A. Curioni, G. Meyer, *New J. Phys.* **12**, 125020 (2010).
18. R. G. Gordon, Y. S. Kim, *J. Chem. Phys.* **56**, 3122 (1972).
19. A. J. Weymouth, T. Hofmann, F. J. Giessibl, *Science* **343**, 1120–1122 (2014).
20. J. C. Slater, *Phys. Rev.* **36**, 57–64 (1930).
21. Supplementary materials are available on *Science* Online.
22. R. Smoluchowski, *Phys. Rev.* **60**, 661–674 (1941).
23. M. Schneiderbauer, M. Emmrich, A. J. Weymouth, F. J. Giessibl, *Phys. Rev. Lett.* **112**, 166102 (2014).
24. M. Feng *et al.*, *ACS Nano* **5**, 8877–8883 (2011).
25. P. Hapala, R. Temirov, F. S. Tautz, P. Jelínek, *Phys. Rev. Lett.* **113**, 226101 (2014).
26. G. Kresse, J. Hafner, *Phys. Rev. B* **47**, 558–561 (1993).
27. M. Huang, M. Čuma, F. Liu, *Phys. Rev. Lett.* **90**, 256101 (2003).
28. L. A. Zotti, W. A. Hofer, F. J. Giessibl, *Chem. Phys. Lett.* **420**, 177–182 (2006).
29. C. A. Wright, S. D. Solares, *Nano Lett.* **11**, 5026–5033 (2011).
30. H. Brune, J. Wintterlin, G. Ertl, R. J. Behm, *Europhys. Lett.* **13**, 123–128 (1990).
31. J. Repp, G. Meyer, K.-H. Rieder, P. Hyldgaard, *Phys. Rev. Lett.* **91**, 206102 (2003).
32. D. M. Eigler, E. K. Schweizer, *Nature* **344**, 524–526 (1990).
33. J. A. Stroscio, R. J. Celotta, *Science* **306**, 242–247 (2004).
34. M. F. Crommie, C. P. Lutz, D. M. Eigler, *Science* **262**, 218–220 (1993).
35. A. Biedermann, W. Rupp, M. Schmid, P. Varga, *Phys. Rev. B* **73**, 165418 (2006).
36. M. Pivetta, G. E. Pacchioni, U. Schlickum, J. V. Barth, H. Brune, *Phys. Rev. Lett.* **110**, 086102 (2013).
37. A. A. Khajetoorians *et al.*, *Science* **339**, 55–59 (2013).
38. B. Schuler *et al.*, *Phys. Rev. Lett.* **111**, 106103 (2013).
39. F. Pielmeier, F. J. Giessibl, *Phys. Rev. Lett.* **110**, 266101 (2013).
40. Our initial experiments of evaporating Fe atoms on Cu(111) appeared to confirm the findings of the inverse of the threefold tip 3 of (*8*), because we found many threefold structures that we first misinterpreted as single atoms. It turned out that upon extended Fe evaporation, the copper crystal heated up to ~15 K and the Fe monomers became mobile enough to form an abundance of trimers.

ACKNOWLEDGMENTS

We thank G. Binnig, J. Repp, and A. J. Weymouth for discussions and the Deutsche Forschungsgemeinschaft for funding under Graduiertenkolleg 1570 and Sonderforschungsbereich 689, as well as M. Grifoni (speaker of GRK) and D. Weiss (speaker of SFB) for support. F.J.G. thanks A. Heinrich for hosting several visits at the IBM Almaden Research Center from 2005 until 2010, where first attempts to resolve metallic adatoms with subatomic resolution were performed together with C. Lutz, C. Hirjibehedin, and M. Ternes. Author contributions: M.E. performed most of the measurements and data analysis, constructed the low-temperature scan head, and prepared most figures; F.H. optimized the electronics and performed crucial measurements; J.W. performed measurements on Cu adatoms on Cu(111); T.H. and F.P. performed measurements on Cu/Cu(110) and inverse measurements using CO/Cu(111) to characterize Cu and Fe tips; M.S. constructed most of the vacuum system and sample-preparation facilities; D.M. performed the AFM measurements on Si; D.K., S.P., S.M., and H.E. performed the DFT calculations; and F.J.G. initiated and directed the project, employed the STO model, and wrote the manuscript.

SUPPLEMENTARY MATERIALS

www.sciencemag.org/content/348/6232/308/suppl/DC1
Materials and Methods
Supplementary Text
Figs. S1 to S13
References (*41*–*47*)

19 December 2014; accepted 20 February 2015
Published online 19 March 2015;
10.1126/science.aaa5329

ACTIVE GALAXIES

A strong magnetic field in the jet base of a supermassive black hole

Ivan Martí-Vidal,* Sébastien Muller, Wouter Vlemmings, Cathy Horellou, Susanne Aalto

Active galactic nuclei (AGN) host some of the most energetic phenomena in the universe. AGN are thought to be powered by accretion of matter onto a rotating disk that surrounds a supermassive black hole. Jet streams can be boosted in energy near the event horizon of the black hole and then flow outward along the rotation axis of the disk. The mechanism that forms such a jet and guides it over scales from a few light-days up to millions of light-years remains uncertain, but magnetic fields are thought to play a critical role. Using the Atacama Large Millimeter/submillimeter Array (ALMA), we have detected a polarization signal (Faraday rotation) related to the strong magnetic field at the jet base of a distant AGN, PKS 1830−211. The amount of Faraday rotation (rotation measure) is proportional to the integral of the magnetic field strength along the line of sight times the density of electrons. The high rotation measures derived suggest magnetic fields of at least tens of Gauss (and possibly considerably higher) on scales of the order of light-days (0.01 parsec) from the black hole.

The AGN jets, related to the accretion mechanism in supermassive black holes, consist of relativistic plasma driven by strong and ordered magnetic fields. As a result of the magnetic interaction of the plasma, nonthermal (synchrotron) emission is produced (*1*). Studying the polarization of this nonthermal emission from AGN is a direct way to probe the structure and strength of magnetic fields in the vicinity of a black hole. Of particular importance is the observation of the rotation measure, *RM*, defined as the change of polarization angle as a function of wavelength squared. This quantity is directly related to the plasma density and the strength of the magnetic field along the line of sight.

To date, it has been extremely difficult to obtain accurate polarimetric information from the innermost (subparsec) regions of AGN; only emission at submillimeter wavelengths can escape from these regions, due to a large synchrotron self-absorption (SSA) that blocks the emission at longer wavelengths. Unfortunately, the sensitivity of polarization observations at submillimeter wavelengths has so far been strongly limited by the instrumentation.

Previous attempts to detect Faraday rotation at submillimeter (submm) wavelengths from AGN have yielded only upper limits (*2*, *3*) and marginal detections (*4*) that require strong assumptions about the absence of variability on time scales of weeks. There is a more robust detection for the Galactic center (*5*), although the activity in this source is much lower than in AGN. Recently, measurements of Faraday rotation in the nearby AGN 3C 84 (redshift z = 0.018) have been reported at mm wavelengths (*6*).

We have obtained measurements of Faraday rotation at frequencies up to 300 GHz (about 1 THz in the rest frame of the source) from PKS 1830−211, a powerful gravitationally lensed AGN located at a redshift of z = 2.5 (*7*). At these frequencies, SSA is negligible in the whole jet of PKS 1830−211 (*8*), and the maximum emission originates at the jet region closest to the black hole; the zone where the plasma is being injected and accelerated into the main jet stream. At lower frequencies, SSA hides this jet acceleration zone

Department of Earth and Space Sciences, Chalmers University of Technology, Onsala Space Observatory, SE-43992, Onsala, Sweden.
*Corresponding author. E-mail: mivan@chalmers.se

from view. These results are thus fundamental to better understand the role of magnetic fields in the AGN accretion and jet production, which are intimately related to the growth and evolution of supermassive black holes.

This detection has been possible thanks to the high resolution (sub-arcsec) of our observations with ALMA and to the use of a new differential polarimetry technique, which we briefly describe in the following lines (see supplementary text section 1).

The ALMA receivers detect the signal in two orthogonal linear polarizations, X and Y, where X is received from a horizontal dipole and Y from a vertical dipole in the frame of the antenna mount. The two lensed images of PKS 1830–211, which we call northeast (NE, upper-left in projection on sky) and southwest (SW, lower-right), are separated by 1″. In Fig. 1, we show an example of snapshot images in XX and YY of the two components of the gravitational lens, as well as their difference. The difference image contains information about the difference between NE and SW in Stokes parameters Q and U. Our analysis makes use of the polarization ratio, $R_{\rm pol}$, which is defined as

$$R_{\rm pol} = \frac{1}{2}\left(\frac{R^{1,2}_{\rm XX}}{R^{1,2}_{\rm YY}} - 1\right)$$

where $R^{1,2}_{\rm XX}$ and $R^{1,2}_{\rm YY}$ are the flux-density ratios between the two lensed images of the AGN, obtained separately from the XX and YY polarization products. $R_{\rm pol}$ is a function of the parallactic angle of the antennas, ψ, and the observing wavelength, λ, and encodes information about the difference of polarization between the two images, via the approximately constant parameters $p_{\rm dif}$ and α (supplementary text section 1), as well as their rotation measure RM,

$$R_{\rm pol} = p_{\rm dif}\cos(2\phi'^{0}_{1} - \alpha + 2RM(\lambda^2 - \psi/RM)) \tag{1}$$

where ϕ'^{0}_{1} is the position angle of the polarization of image 1 at zero wavelength in the plane of the sky. The technique of differential polarimetry essentially enables estimation of RM via fitting the observed sinusoidal dependence of $R_{\rm pol}$ as a function of λ^2 and ψ, using Eq. 1.

Our results are based on ALMA observations at sky frequencies around 100, 250, and 300 GHz (*8*). Correcting for the cosmological redshift, these frequencies correspond to 350, 875, and 1050 GHz

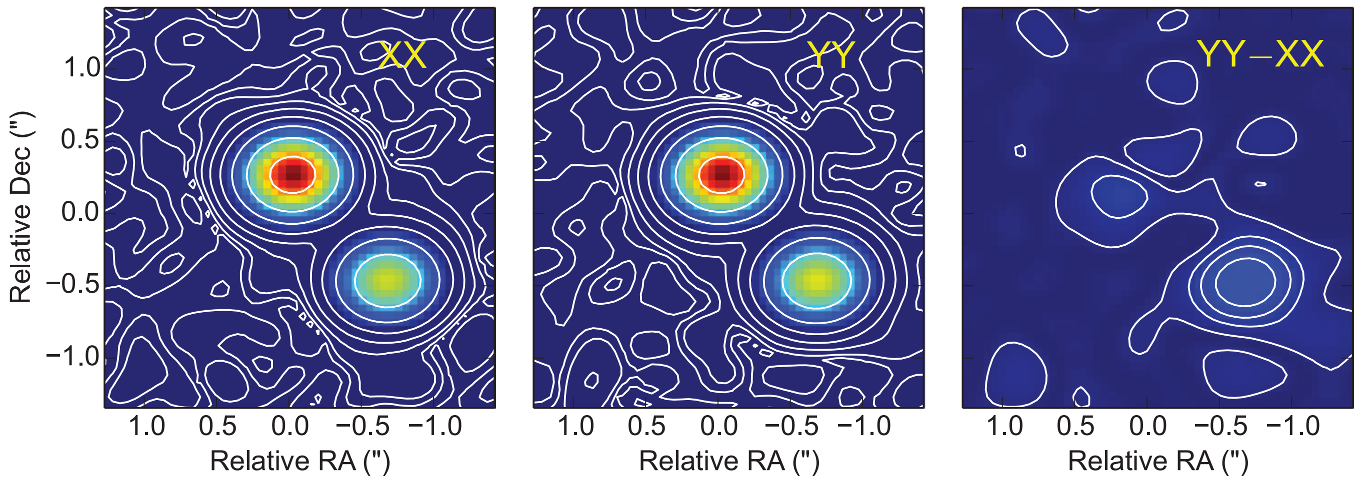

Fig. 1. ALMA image of the gravitationally lensed AGN PKS 1830−211 at 250 GHz, taken on 30 June 2014. Left, in XX polarization; center, in YY polarization (with the peak normalized to that of the XX image); right, the difference between polarizations. Notice the small residual in the southwest lensed image, which encodes differential polarization information among the northeast and southwest images. The contours are set at 0.625, 1.25, 2.5, 5, 10, 20, 50, and 99% of the peak intensity.

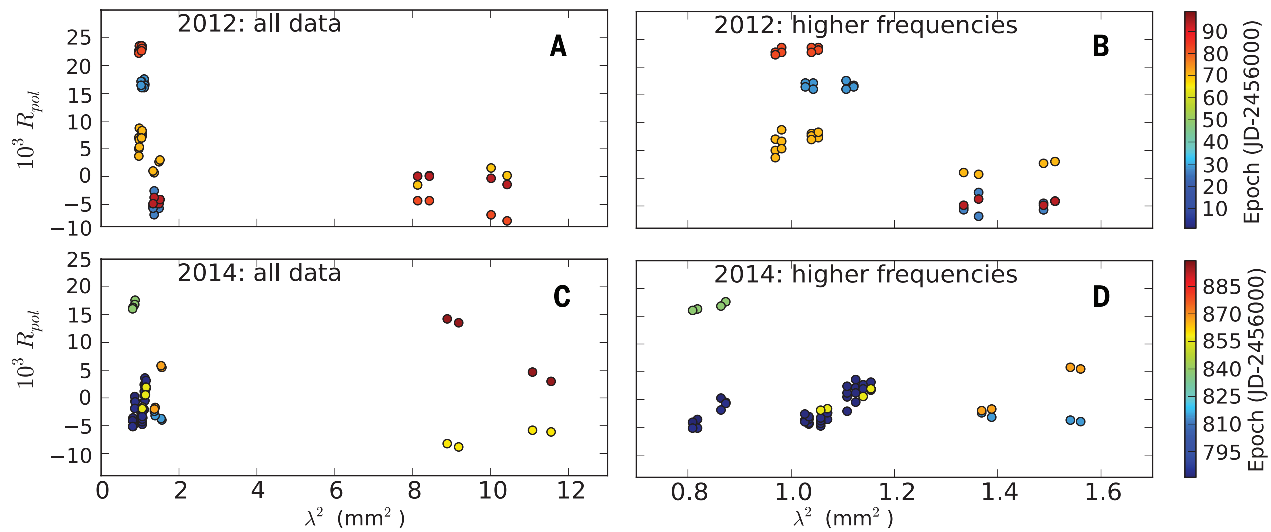

Fig. 2. Polarization ratio, $R_{\rm pol}$, as a function of the wavelength squared for all our ALMA observations. Left panels (**A** and **C**) are all data; right panels (**B** and **D**) are enlargements of the region of shorter wavelengths. The uncertainties, estimated from the postfit covariance matrix as described in (*10*), are of the order of the symbol sizes.

in the frame of the source. More details on these observations, and a summary of the main goals of this ALMA project, can be found elsewhere (*9*). We also summarize all the observations in the supplementary text (section 2). Our observations can be divided in two data sets, one consisting of six epochs in 2012 (9 April to 16 June) and the other of nine epochs in 2014 (3 May to 27 August). In Fig. 2, we show the measured R_{pol} between the two lensed images of PKS 1830–211. These measurements have been obtained from the R_{XX} and R_{YY} values fitted with the visibility-modeling software presented in (*10*). The uncertainties have been obtained with the standard error propagation approach, using the uncertainties in R_{XX} and R_{YY} that were derived from the covariance matrix of the visibility fitting, as described in (*10*).

The derivatives of R_{pol} versus λ^2, which are related to *RM* (supplementary text section 1.3), are clearly different for different wavelength ranges. Between λ^2 = 8 and 12 mm^2, the maximum derivative is 4.4 × 10^{-3} mm^{-2}, whereas between 0.8 and 1.6 mm^2 it is 70 × 10^{-3} mm^{-2}. Because the maximum observed R_{pol} ratios are, in absolute value, similar at all wavelengths, the different derivatives of R_{pol} versus λ^2 must be due to larger *RM* at shorter wavelengths (see supplementary text section 1.3 for a more detailed discussion). Large variations of *RM* with wavelength have been reported in other AGN (*11*), although at much longer wavelengths (cm), related to larger spatial scales in the jets. Our finding cannot be explained easily if the *RM* is only caused by an external (e.g., spherically symmetric) screen of material being accreted onto the black hole [as in the case of the *RM* detected in the Galactic center (*5*)] and/or by external clouds. The size of the submm emitting region (estimated as the distance to the black hole at which the submm intensity is maximum) is only of the order of 0.01 pc (*8*). Hence, if the Faraday screen were extended and located far from the jet base, the rotation measure at submm wavelengths should not depend on the observing frequency, because the extent of the Faraday screen would be similar for all the submm jet emission. The Faraday screen must thus be close to the jet base and change substantially on sub-parsec scales (Fig. 3). An increase of the *RM* at shorter wavelengths would then be explained naturally as an increase of the magnetic field strength and/or electron density as we approach the black hole. Indeed, observations of other AGN at long wavelengths (cm) show changes of *RM* across the jets, both longitudinal and transversal (*12*–*14*), that have been attributed to changes in particle density and magnetic fields in the jets, independent of a more distant external medium.

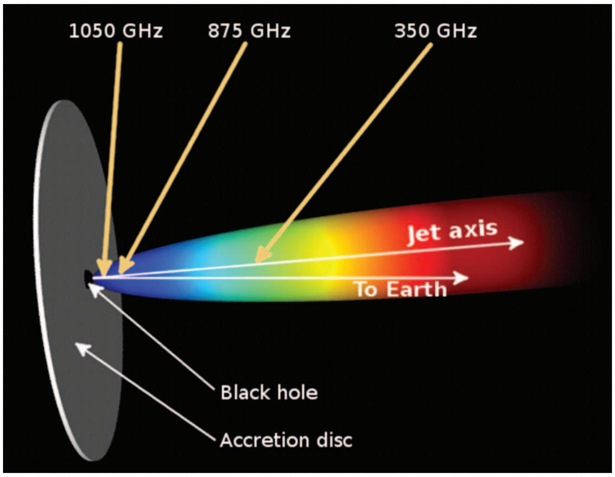

Fig. 3. Sketch of the jet launch/acceleration region in PKS 1830–211 (not to scale). Emission at higher frequencies comes from material closer to the black hole, at subparsec scales. At these frequencies, the main contribution to *RM* must come from a zone close to the jet, in order to explain the different *RM* values between 350 GHz and 0.8 to 1 THz (source frame).

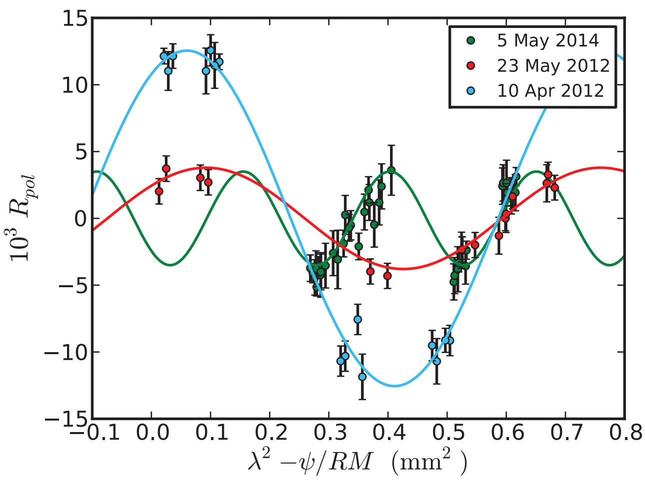

Fig. 4. Fits of our three epochs with quasi-simultaneous observations at 250 and 300 GHz to the model given in Eq. 1. We show R_{pol} versus λ^2 corrected by $-\psi/RM$, to obtain a sinusoidal behavior.

We have three sets of observing epochs at 250 and 300 GHz separated by a short time interval (1 to 2 days). In these three cases, we can directly estimate *RM* and p_{dif} by fitting R_{pol} to the model given by Eq. 1. The parameter estimates in these three data sets have been performed by least-squares minimization, comparing the measured R_{pol} to the model predictions. The data at our lowest-frequency band (i.e., 100 GHz) have been discarded from the fit, because they trace different rotation measures from different regions of the jet, as we have already discussed. We show the fitting results in Fig. 4 and the estimated parameters in Table 1. Our estimated source–rest-frame *RM*s are about two orders of magnitude higher than the highest values reported previously for other AGN, which are ~10^6 rad/m^2 (*4*, *6*).

Although the two *RM* measurements in 2012 are compatible, the estimate in 2014 is higher by more than a factor of 2. Regarding the amplitude of R_{pol}, which is related to the fractional polarization and to the relative polarization angles among the NE and SW images, we find different values for the two observations in 2012. These two observations were serendipitously taken before and after a strong γ-ray flare, which had a very weak radio counterpart (*8*). This leads us to speculate that the change in polarization may be correlated to the radio counterpart of that flare. Another γ-ray flare was detected in 2014 (*15*), also coincident with the time range of our 2014 observations. The new flare had a strong radio counterpart, which may also be related to the higher *RM* that we measure in 2014. The high variability in *RM* and p_{dif}, in connection to the γ-ray flaring events, points toward a cospatial origin of the γ-ray emission and the 250- to 300-GHz rotation measures, hence favoring our interpretation of the *RM* being caused at the region very close to the jet base.

Table 1. Best-fit polarization values for the three epochs with quasi-simultaneous observations at 250 and 300 GHz. RM_{obs} are the rotation measures in the observer's frame and RM_{true} are the rotation measures in the rest frame of the source. RM_{true} is $(1+z)^2$ times larger than RM_{obs}.

	Epoch		
	10 April 2012	23 May 2012	5 May 2014
RM_{obs} (10^6 rad/m^2)	9.0 ± 0.3	9.4 ± 0.4	25.3 ± 0.8
RM_{true} (10^7 rad/m^2)	11 ± 0.4	11.5 ± 0.5	31.2 ± 1.0
p_{dif} (10^{-3})	12.6 ± 0.4	3.8 ± 0.3	3.5 ± 0.3
$2\phi_0 - \alpha$ (deg)	59 ± 27	40 ± 23	25 ± 20

The *RM* is related to the line-of-sight integral of the electron density times the magnetic field, corrected for the cosmological redshift (*16*). In units of rad/m^2,

$$RM = 8.1 \times 10^5 \frac{1}{(1+z)^2} \int n\, B_{||} dl \qquad (2)$$

where dl is the differential path along the line of sight (in pc), z is the redshift (z = 2.5), n is the particle density (in cm^{-3}), and $B_{||}$ is the magnetic field projected in the line of sight (in Gauss). Our *RM* will be an important test for detailed magnetohydrodynamical (MHD) models at the jet base, but such analysis is beyond the scope of this paper. At a more basic level, it is impossible to unambiguously disentangle the contributions of the magnetic field, electron density, and path length to the integral determining the rotation measure. This difficulty is exacerbated by the absence of direct information about the electron density or path length from observations, leading to the need to extrapolate from larger scales, which introduces additional uncertainty. The rotation measures derived here, $RM \sim 10^8$ rad/m^2 in the rest frame of the source, are about a factor of 10^5 greater than the rest-frame *RM* values measured for parsec-scale AGN cores, where the derived magnetic fields have been independently measured to be ~0.05 to 0.10 G (*11*, *17*); this suggests that the magnetic fields in the subparsec regions that we are probing are at least a few tens of Gauss, and possibly much higher. More exact estimates of these magnetic fields will require a separate dedicated study.

In any case, our results are a clear indication of very high magnetic fields at the jet base, which should be dynamically important near the black hole and should in turn affect the accretion process. A similar conclusion was drawn from a statistical analysis of jet core shifts from a complete sample of AGN, using high-resolution radio observations at centimeter wavelengths (*18*). In the near future, our differential polarimetry technique can be used to further measure and monitor *RM*s at very short wavelengths, from this and other AGN. The monitoring of magnetic fields and particle densities at the jet regions closest to the black holes, via submm polarimetry, will allow us to study the tight connection between black-hole accretion and relativistic jets, the two fundamental pieces of the fascinating cosmic puzzle of AGN.

REFERENCES AND NOTES

1. A. P. Marscher, *Astrophys. J.* **235**, 386 (1980).
2. I. Agudo, C. Thum, J. L. Gómez, H. Wiesemeyer, *Astron. Astrophys.* **566**, A59 (2014).
3. C. Y. Kuo, K. Asada, R. Rao, M. Nakamura, J. C. Algaba, H. B. Liu, M. Inoue, P. M. Koch, P. T. P. Ho, S. Matsushita, H.-Y. Pu, K. Akiyama, H. Nishioka, N. Pradel, *Astron. Astrophys.* **783**, 33 (2014).
4. S. Trippe *et al.*, *Astron. Astrophys.* **540**, A74 (2012).
5. D. P. Marrone, J. M. Moran, J.-H. Zhao, R. Rao, *Astrophys. J.* **654**, L57–L60 (2007).
6. R. L. Plambeck *et al.*, *Astrophys. J.* **797**, 66 (2014).
7. C. Lidman *et al.*, *Astrophys. J.* **514**, L57–L60 (1999).
8. I. Martí-Vidal *et al.*, *Astron. Astrophys.* **558**, A123 (2013).
9. S. Muller *et al.*, *Astron. Astrophys.* **566**, A112 (2014).
10. I. Martí-Vidal, W. Vlemmings, S. Muller, S. Casey, *Astron. Astrophys.* **563**, A136 (2014).
11. S. P. O'Sullivan, D. C. Gabuzda, *Mon. Not. R. Astron. Soc.* **393**, 429–456 (2009).
12. S. M. Croke, S. P. O'Sullivan, D. C. Gabuzda, *Mon. Not. R. Astron. Soc.* **402**, 259–270 (2010).
13. M. Mahmud, D. Gabuzda, V. Bezrukovs, *Mon. Not. R. Astron. Soc.* **400**, 2–12 (2009).
14. D. C. Gabuzda, V. A. Chernetskii, *Mon. Not. R. Astron. Soc.* **339**, 669–679 (2003).
15. S. Ciprini, *The Astronomers Telegram* **4158** (2012).
16. M. L. Bernet, F. Miniati, S. Lilly, *Astrophys. J.* **761**, 144 (2012).
17. S. P. O'Sullivan, D. C. Gabuzda, *Mon. Not. R. Astron. Soc.* **400**, 26–42 (2009).
18. M. Zamaninasab, E. Clausen-Brown, T. Savolainen, A. Tchekhovskoy, *Nature* **510**, 126–128 (2014).

ACKNOWLEDGMENTS

This paper makes use of the following ALMA data: ADS/JAO.ALMA#2011.0.00405.S, ADS/JAO.ALMA#2012.1.00056.S, and ADS/JAO.ALMA#2013.1.00020.S. ALMA is a partnership of the European Southern Observatory (ESO) (representing its member states), U.S. National Science Foundation (NSF), and National Institutes of Natural Sciences (NINS) of Japan, together with the National Research Council of Canada (NRC) and National Science Council of Taiwan (NSC) and Academia Sinica Institute of Astronomy and Astrophysics (ASIAA) (Taiwan), in cooperation with the Republic of Chile. The Joint ALMA Observatory is operated by ESO, Associated Universities, Inc.–National Radio Astronomy Observatory, and National Astronomical Observatory of Japan. W.V. acknowledges support from the European Research Council (ERC) under ERC grant 614264.

SUPPLEMENTARY MATERIALS

www.sciencemag.org/content/348/6232/311/suppl/DC1
Supplementary Text
Figs. S1 to S4
Tables S1 to S3
Reference (*19*)

28 October 2014; accepted 12 March 2015
10.1126/science.aaa1784

GALAXY EVOLUTION

Evidence for mature bulges and an inside-out quenching phase 3 billion years after the Big Bang

S. Tacchella,[1]* C. M. Carollo,[1]* A. Renzini,[2] N. M. Förster Schreiber,[3] P. Lang,[3] S. Wuyts,[3] G. Cresci,[4] A. Dekel,[5] R. Genzel,[3,6,7] S. J. Lilly,[1] C. Mancini,[2] S. Newman,[6] M. Onodera,[1] A. Shapley,[8] L. Tacconi,[3] J. Woo,[1] G. Zamorani[9]

Most present-day galaxies with stellar masses ≥10^{11} solar masses show no ongoing star formation and are dense spheroids. Ten billion years ago, similarly massive galaxies were typically forming stars at rates of hundreds solar masses per year. It is debated how star formation ceased, on which time scales, and how this "quenching" relates to the emergence of dense spheroids. We measured stellar mass and star-formation rate surface density distributions in star-forming galaxies at redshift 2.2 with ~1-kiloparsec resolution. We find that, in the most massive galaxies, star formation is quenched from the inside out, on time scales less than 1 billion years in the inner regions, up to a few billion years in the outer disks. These galaxies sustain high star-formation activity at large radii, while hosting fully grown and already quenched bulges in their cores.

At the epoch when star-formation activity peaks in the universe [redshift $z \sim 2$ (*1*, *2*)], massive galaxies typically lie on the so-called "star-forming main sequence." Their star-formation rates (SFRs) tightly correlate with the mass in stars (stellar mass M), reaching up to several hundred solar masses ($M_\odot$) per year and producing a characteristic specific SFR (sSFR = SFR/M) that declines only weakly with mass (*3*, *4*). In contrast, at the present epoch, such massive galaxies are spheroids with old stellar populations, which reach central surface stellar densities well above 10^{10} $M_\odot$ kpc^{-2} and host virtually no ongoing star formation. Although the most massive ellipticals at z = 0 bear the clear signatures of a gas-poor formation process (*5*, *6*), the more typical population, at a mass scale of $M \sim 10^{11}$ $M_\odot$, consists of fast rotators (*7*) with disk-like isophotes (*8*), steep nuclear light profiles (*9*), and steep metallicity gradients (*10*): all features that indicate a gas-rich formation process.

The full cessation of star-formation activity in these typical massive galaxies (here referred to as the quenching process) is not well understood, nor is its relation with the emergence of their spheroidal morphologies. Several quenching mechanisms have been proposed. The so-called halo-quenching scenario predicts that circumgalactic gas is shock-heated to high temperatures and

[1]Department of Physics, Institute for Astronomy, ETH Zurich, CH-8093 Zurich, Switzerland. [2]Istituto Nazionale di Astrofisica (INAF) Osservatorio Astronomico di Padova, Vicolo dell Osservatorio 5, I-35122 Padova, Italy. [3]Max-Planck-Institut für Extraterrestrische Physik, Giessenbachstrasse 1, D-85748 Garching, Germany. [4]INAF Osservatorio Astronomico di Arcetri, Largo Enrico Fermi 5, I-50125 Firenze, Italy. [5]Racah Institute of Physics, The Hebrew University, Jerusalem 91904, Israel. [6]Department of Astronomy, Campbell Hall, University of California, Berkeley, CA 94720, USA. [7]Department of Physics, Le Conte Hall, University of California, Berkeley, CA 94720, USA. [8]Department of Physics and Astronomy, University of California, Los Angeles, CA 90095-1547, USA. [9]INAF Osservatorio Astronomico di Bologna, Via Ranzani 1, I-40127 Bologna, Italy.
***Corresponding author. E-mail: sandro.tacchella@phys.ethz.ch (S.T.); marcella.carollo@phys.ethz.ch (C.M.C.)**